SCEC Project 20204 – Final Technical Report

Dynamic Rupture Modeling of Coseismic Interactions on Orthogonal Strike-Slip Faults

Julian Lozos (California State University, Northridge)

Introduction

Strike-slip fault systems are classified by the sense of slip of their primary faults. Orthogonal faults with the opposite sense of slip can exist in such systems, particularly in transpressional or transtensional settings (Thatcher & Hill, 1991). Where two orthogonal faults cross, the issue of them rupturing together arises. The opposite senses of slip makes fault interactions more complex here, and the geometry of a cross-fault system has many possible paths for a multifault rupture.

There are three categories of orthogonal fault ruptures: (a) one fault ruptures, but the second remains uninvolved, (b) a rupture begins on one fault and propagates onto the other, or (c) one fault ruptures, then the second ruptures during the postseismic period of the first. California examples for the first category include the M7.3 1992 Landers earthquake, which crossed the Pinto Mountain Fault without activating it (Hauksson et al., 1993); for the second category, the 1992 M6.5 Big Bear, California (Jones et al., 1993); and for the third category, the 2019 Ridgecrest, California sequence, in which a M6.4 was followed by a M7.1 on an orthogonal fault the next day (Ross et al., 2019).

The orthogonal fault question is an earthquake gate question: what allows rupture to propagate through both faults, versus confining rupture to one or the other? Dynamic rupture modeling is ideal for addressing this question, since it allows exploration of initial conditions, and since the physics of rupture determines the outcome. There are many previous dynamic rupture modeling studies that explore what controls rupture behavior at earthquake gates. For orthogonal geometries in general, two consider dip-slip faults (Magistrale & Day, 1999; Oglesby, 2005), and others focus on specific orthogonal strike-slip fault systems or earthquakes (e.g., Cortez et al., 2021; Kyriakopoulos et al., 2019; Lozos & Harris, 2020). Here, I simulate nonspecific ruptures on generic strike-slip faults, to explore the basic physics of how rupture negotiates orthogonal fault geometry.

Methods and Model Setup

I use the 3-D finite element software FaultMod (Barall, 2009), which performs consistently in the SCEC Dynamic Rupture Code Verification Exercise (Harris et al., 2018) to conduct dynamic rupture simulations on orthogonal strike-slip fault systems in a homogeneous elastic half space. I implement linear slip-weakening friction (Andrews, 1976; Ida, 1972), and I nucleate ruptures at the end of each branch of the fault system by raising shear stress over the yield stress, then forcing propagation over an area larger than the critical patch size required for self-sustaining rupture (Day, 1982). My physical parameters are taken from the classic dynamic rupture modeling study Harris and Day (1993).

I generated meshes of vertical strike-slip faults with 12 km basal depth using the commercial software Trelis. I created two T-shaped strike-slip fault geometries: both with one 60 km-long north-south-oriented fault, and a 30-km long east-west-oriented fault that branches to one side of the first fault at its midpoint. Because FaultMod requires that one fault be discontinuous at an intersection, also created two +-shaped geometries, each with two 60 km-long faults: one where the NS fault is continuous and the EW one is discontinuous at the junction, and vice-versa.

I test two initial stress cases: one with higher shear and normal stresses and higher strength (S) (Das & Aki, 1977), and one with lower overall stresses, lower S. In uniform traction models, I directly assign one of these stress cases to each fault. In regional stress models, I resolve principal stresses equivalent to one of the stress cases onto both faults. Initial on-fault tractions depend on the angle between the faults and the maximum horizontal compressive stress (S_{Hmax}).

Results

Rupture Behaviors

My models produce five rupture patterns, all of which occur in both high- and low-stress cases:

Single-fault. Rupture propagates through the entire nucleation fault, but the cross fault does not activate.

Multi-fault. Rupture propagates through the entire nucleation fault and at least part of the cross fault.

Triggered slip. The nucleation fault hosts a propagating rupture front and ruptures completely. The cross fault sustains a small patch of triggered slip near the junction.

Triggered nucleation. Under some regional stress conditions, the nucleation fault is too unfavorable for rupture. However, the cross fault is so favorable that stress changes from the failed forced nucleation trigger rupture on the cross fault.

Failed nucleation. The nucleation fault is too unfavorable to rupture, and its effect on the cross fault is too small to nucleate a secondary rupture.

Figure 1

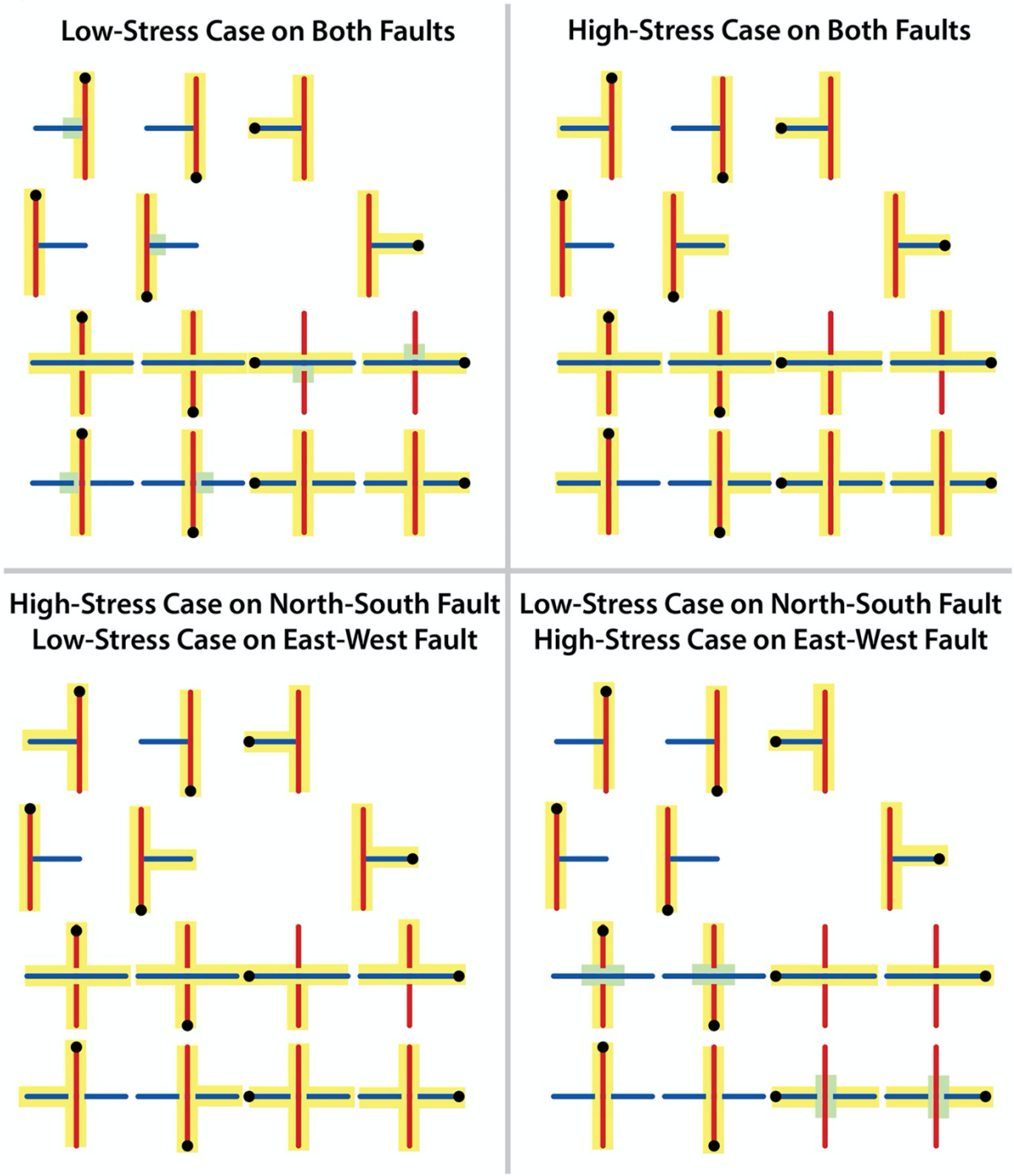

Figure 1. Rupture patterns for uniform traction models. Red lines are right-lateral faults, blue lines are left-lateral faults. The black dot marks the nucleation. Faults that ruptured in each model are highlighted in yellow; triggered slip is highlighted in green.

Uniform Traction Models

In all combinations of stress cases across all geometries, some multifault ruptures occur: particularly when the nucleation fault ends or is discontinuous at the junction (Figure 1). When both faults have the same initial tractions, the nucleation point effectively controls the rupture pattern, because it determines the direction of motion and the pattern of stress changes toward the junction. Regardless of nucleation point, more multifault ruptures occur with the high-stress (subshear) case on both faults, despite its higher strength (S) and slower rupture velocity than the low-stress (supershear) case. This is because the higher yield stress produces a higher dynamic stress drop and a higher-energy rupture front that more easily propagates through geometrical complexities.

When the high-stress case is on one fault and the low-stress case is on the other, the high-stress fault dominates the rupture. Ruptures that nucleate on high-stress faults propagate onto low-stress faults as if they were also high-stress faults. Meanwhile, ruptures that nucleate on low-stress faults do not propagate onto high-stress faults unless the low-stress fault ends at the high-stress one, because the stresses from these ruptures are too low to exceed the higher yield stress without the help of increased shear stress from a stopping phase.

Regional Stress Models

As expected, S_{Hmax} = N45°E models were identical to uniform traction models where both faults have the same initial stresses. I next tested S_{Hmax} of 30° away from either fault: the optimal angle for conjugate strike-slip faults (Anderson, 1951; Jaeger & Cook, 1979). However, under these conditions, no multifault ruptures occurred. If nucleation is on the more favorable fault, rupture remains on that fault. If nucleation is on the less-favorable fault, rupture stops after forced nucleation. If one fault is significantly more favorable but nucleation is on the other, rupture on the first fault stops, but seismic waves from the forced nucleation trigger a secondary rupture at the junction, which propagates through the cross fault. It is, however, implausible that orthogonal faults would form under the stress conditions required for this rupture pattern (Anderson, 1951; Thatcher & Hill, 1991).

Since the optimal S_{Hmax} for conjugate faulting did not produce multifault rupture, I kept rotating S_{Hmax} until both faults ruptured together. For the high-stress (subshear) case, S_{Hmax} needed to be 43°–45° away from either fault, with S on either fault no larger than 2.79. The range for the low-stress (supershear) case was wider: 34°–45° from either fault, with maximum S of 1.92.

Discussion

Fault Geometry Effects

Uniform traction models with the same stresses on both faults isolate the effects of the fault geometry. The primary geometrical effects on rupture pattern come from the initial direction of slip toward the second fault.

Figure 2 illustrates this effect. In Figure 2a, right-lateral slip initially compresses the left-lateral cross fault, increasing normal stress. Once the rupture front reaches the extensional quadrant south of the junction, shear stress near the junction has already dropped, and is not high enough to allow slip on the cross fault, even under extension–confining rupture to one fault. In Figure 2b, extension acts on the left-lateral cross fault first, reducing its normal stress as the high-shear-stress rupture front approaches. This allows the second fault to begin rupturing before compression activates, and leads to a full rupture of both faults. This is consistent with simulations of non-orthogonal strike-slip junctions, in which rupture also prefers extensional branches over compressional ones (Aochi et al., 2002; Fliss et al., 2005; Kame et al., 2003), as well as with site-specific orthogonal faulting models (Cortez et al., 2021; Kyriakopoulos et al., 2019). This pattern of extension and compression occurs regardless of rupture velocity, which is why supershear and subshear conditions produce very similar rupture patterns across geometrical parameter space.

In T-shaped systems, if rupture begins on the long fault, compression and extension determine whether the short fault can rupture. If the short fault ruptures first, it compresses the long fault on one side of the junction and extends it on the other. However, when rupture reaches the end of the first fault, it produces a high-shear-stress stopping phase that is strong enough to overcome any dynamic compression (Figure 2c). Rupture progresses faster on the extensional side and slower on the compressional one, but all model ruptures which nucleate on the short fault of T-shaped systems propagate onto the second fault for this reason. Similar stopping phases have been identified in seismic data (e.g., Savage, 1965), and secondary nucleations caused by stopping phases also occur in simulations of fault stepovers (e.g., Oglesby, 2008) and bends (e.g., Lozos et al., 2011).

Figure 2.

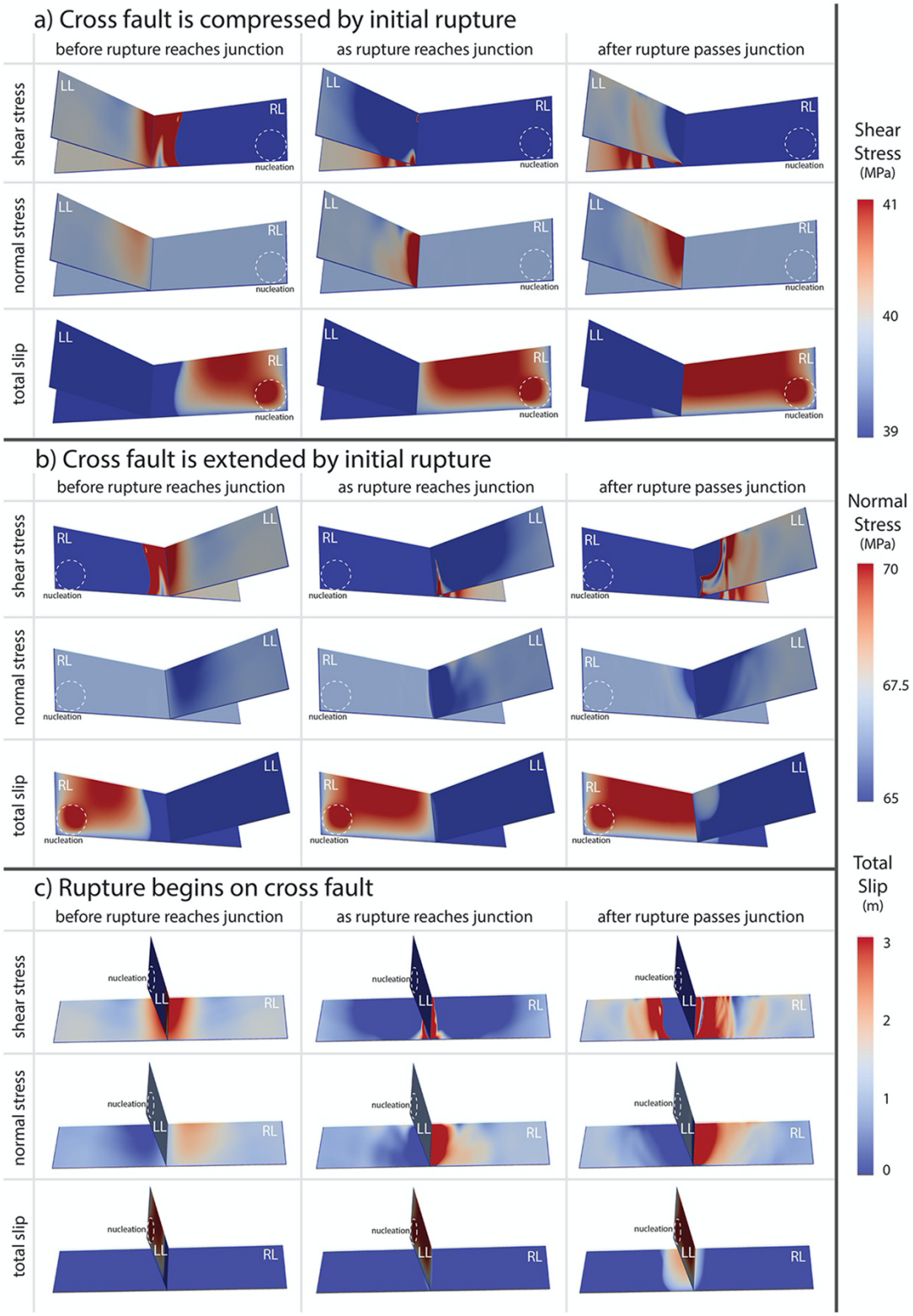

Figure 2. Stress effects of initial rupture directions. Top: the cross fault is compressed first, which prevents multi-fault rupture. Center: the cross fault is extended first, which allows rupture to propagate through both faults. Bottom: a high-shear-stress stopping phase allows bilateral rupture on the long fault.

These extension and compression effects apply in +-shaped systems, where one fault is discontinuous at the junction. A rupture on the continuous fault causes either rupture or triggered slip on the extensional side of the cross fault (while the compressional side does not activate). A rupture on the discontinuous fault will cause either rupture or triggered slip on both sides of the cross fault, due to extension on one side, and to the high-shear-stress stopping phase overcoming compression on the other: an effect that is analogous to rupture jumping a stepover (Oglesby, 2008). This also agrees with simulations of nonorthogonal splays which show that rupture jumps from one fault to another if they are mutually discontinuous at the junction, regardless of compression or extension (DeDontney et al., 2012).

Stress Level Effects

Under uniform traction, absolute stresses on both faults affect whether multifault rupture occurs, even if both faults are individually favorable for failure. This is not an effect of fault strength (S), but rather how high the stresses on one fault are relative to the other. A rupture on a lower-stress fault will not propagate onto a higher-stress fault, since neither a normal stress reduction from dynamic unclamping, nor a shear stress increase from a stopping phase, can overcome the yield stress on the high-stress fault. Similarly, a rupture which starts on a lower-stress fault needs a stopping phase to initiate rupture on another low-stress fault. Rupture can propagate from a higher-stress fault onto a lower-stress fault, since the shear stress on the high-stress fault is closer to the yield stress of the lower-stress fault. In these cases, rupture patterns follow the same geometrical controls as if both faults had high stresses. Other modeling studies on rupture through geometrical complexities show similar interactions between high- and low-stress faults (e.g., Duan & Oglesby, 2006; Kame et al., 2003; Lozos et al., 2011).

When I rotate S_{Hmax} to 30° from either fault, one becomes significantly less favorable for rupture than the other, both in terms of individual fault strength (S) and relative shear stress. This prevents multifault ruptures across my entire geometrical parameter space, regardless of dynamic extension or compression; rupture cannot even nucleate on the less-favorable fault, despite being forced. Triggered slip or nucleation on the more-favorable fault follows the same geometrical and kinematic rules for multifault rupture described above.

That the low-stress case allows multi-fault ruptures over a wider range of S_{Hmax} than in the high-stress case is predominantly a normal-stress effect (e.g., Lozos et al., 2011). Rotating S_{Hmax} can increase normal stress relative to shear stress in either case; because the overall levels are lower in the low-stress case, the absolute amount that shear stress must increase to exceed the yield stress is still less than in the high-stress case (e.g., Harris & Day, 1993; Oglesby, 2005; Lozos et al., 2014). The high-shear-stress stopping phase in particular is what allows multifault ruptures at larger S_{Hmax} deviations from 45° in the low-stress case.

Implications and Conclusions

Stresses on the cross fault of an orthogonal strike-slip fault system–and how high or low they are compared to stresses on the nucleating fault–control whether multi-fault rupture occurs. If the second fault is not favorable for rupture on its own, it will not rupture, regardless of the effects of rupture on the first fault. Many factors affect real-world stress accumulation, but within the uniform stress fields of my simulations, only a narrow range of S_{Hmax}, close to 45° from either fault, allows multifault rupture. This is consistent with observations and theory showing that orthogonal faults are most likely to form at 45° from S_{Hmax} (Thatcher & Hill, 1991).

If both faults are favorable for rupture, the nucleation location, and therefore the initial sense of slip toward the second fault, controls whether the second fault can rupture. If the cross fault is extended by the initial movement of the first fault, it is more likely to rupture than if it is compressed. Even when the sense of slip brings the second fault further from failure, a stopping phase from rupture hitting the end of the first fault can still cause the second fault to fail.

Although these models are less complex than real-world earthquakes, the behaviors I show here are consistent with the rupture patterns of many real events (e.g., Hudnut et al., 1989; Jones et al., 1993; Lozos & Harris, 2020; Matsu'ura et al., 1977; Meng et al., 2012; Yue et al., 2012; Cortez et al., 2021). The results of this parameter study may therefore be useful both for interpreting the rupture patterns of historic or paleoseismic earthquakes, and for providing physics-based guidelines for assessing rupture hazard on orthogonal strike-slip fault systems.

Published Manuscript (SCEC publication Database #13427)
Lozos, J. C. (2022). Dynamic rupture modeling of coseismic interactions on orthogonal strike-slip faults. *Geophysical Research Letters*, *49*(5), e2021GL097585.

References Cited

Anderson, E.M. (1951). The dynamics of faulting: Edinburgh, Oliver and Boyd, 206 p

Andrews, D. J. (1976). Rupture propagation with finite stress in antiplane strain, J. Geophys. Res. 81(20), 3575–3582.

Aochi, H., Madariaga, R., & Fukuyama, E. (2002). Effect of normal stress during rupture propagation along nonplanar faults. Journal of Geophysical Research: Solid Earth, 107(B2).

Barall, M. (2009), A grid-doubling finite-element technique for calculating dynamic three-dimensional spontaneous rupture on an earthquake fault. Geophys. Journ. Int., 178, 845-859, doi:10.1111/j.1365-246X.2009.04190.x

Cortez, J. T., D. D. Oglesby, C. Kyriakopoulos, B. Wu, K. Chaudhuri, A. Ghosh, and R. Douilly (2021). On the rupture propagation of the 2019 M6.4 Searles Valley, California, Earthquake, and the lack of immediate triggering of the M7.1 Ridgecrest Earthquake. Geophysical Research Letters, 48(4), e2020GL090659.

Das, S. and Aki, K. (1977). A numerical study of two-dimensional spontaneous rupture propagation. *Geophysical journal international*, *50*(3), pp.643-668.

Day, S. M. (1982). Three-dimensional simulation of spontaneous rupture: The effect of nonuniform prestress, Bull. Seism. Soc. Am. 72(6), 1881–1902.

DeDontney, N., Rice, J.R., and Dmowska, R., 2012, Finite element modeling of branched ruptures including off-fault plasticity: Bulletin of the Seismological Society of America, v. 102, p. 541–562, https://doi.org/10.1785/0120110134.

Duan, B. and Oglesby, D.D., 2006. Heterogeneous fault stresses from previous earthquakes and the effect on dynamics of parallel strike-slip faults. *Journal of Geophysical Research: Solid Earth*, *111*(B5).

Fliss, S., H. S. Bhat, R. Dmowska, and J. R. Rice (2005). Fault branching and rupture directivity: Journal of Geophysical Research: Solid Earth, v. 110(B6), doi:10.1029/2004JB003368.

Harris, R. A. and S. M. Day (1993). Dynamics of fault interaction: Parallel strike-slip faults: Journal of Geophysical Research: Solid Earth, v. 98(B3), p. 4461-4472, doi:10.1029/92JB02272.

Harris, R. A., M. Barall, B. Aagaard, S. Ma, D. Roten, K. Olsen, B. Duan, B. Luo, D. Liu, K. Bai, J.-P. Ampuero, Y. Kaneko, A.-A. Gabriel, K. Duru, T. Ulrich, S. Wollherr, Z. Shi, E. Dunham, S. Bydlon, Z. Zhang, X. Chen, S. N. Somala, C. Pelties, J. Tago, V. M. Cruz-Atienza, J. Kozdon, E. Daub, K. Aslam, Y. Kase, K. Withers, and L. Dalguer (2018). A suite of exercises for verifying dynamic earthquake rupture codes, Seism. Res. Lett., 89(3), 1146-1162, doi:10.1785/0220170222.

Hauksson, E., L. M. Jones, K. Hutton, and D. Eberhart-Phillips. (1993). The 1992 Landers earthquake sequence: Seismological observations. Journal of Geophysical Research: Solid Earth, 98(B11), 19835-19858.

Hudnut, K. W., L. Seeber, and J. Pacheco (1989). Cross-fault triggering in the November 1987 Superstition Hills earthquake sequence, southern California. Geophysical Research Letters, 16(2), 199-202.

Ida, Y. (1972). Cohesive force across the tip of a longitudinal-shear crack and Griffith's specific surface energy, J. Geophys. Res. 77(20), 3796–3805, doi:10.1029/JB077i020p03796.

Jaeger, J. G., and N. G. W. Cook (1979). Fundamentals of rock mechanics (third edition): London, Chapman and Hall, 585 p.

Jones, L. E., S. E. Hough, and D. V. Helmberger (1993). Rupture process of the June 28, 1992 Big Bear earthquake. Geophysical research letters, 20(18), 1907-1910.

Kame, N., J. R. Rice, and R. Dmowska (2003). Effects of prestress state and rupture velocity on dynamic fault branching: Journal of Geophysical Research: Solid Earth, v. 108(B5), doi:10.1029/2002JB002189.

Kyriakopoulos, C., Oglesby, D., Rockwell, T., Meltzner, A., Barall, M., Fletcher, J. M., & Tulanowski, D. (2019). Dynamic rupture scenarios in the Brawley seismic zone, Salton Trough, Southern California. Journal of Geophysical Research: Solid Earth, 124(4), 3680–3707

Lozos, J. C., D. D. Oglesby, B. Duan, and S. G. Wesnousky (2011). The effects of double fault bends on rupture propagation: A geometrical parameter study: Bulletin of the Seismological Society of America, v. 101(1), p. 385-398, doi:10.1785/0120100029.

Lozos, J. C., D. D. Oglesby, J. N. Brune, and K. B. Olsen (2012). Small intermediate fault segments can either aid or hinder rupture propagation at stepovers: Geophysical Research Letters, v. 39(18), doi:10.1029/2012GL053005.

Lozos, J. C., Dieterich, J. H., & Oglesby, D. D. (2014). The effects of d 0 on rupture propagation on fault stepovers. *Bulletin of the Seismological Society of America*, *104*(4), 1947-1953.

Lozos, J. C., and R. A. Harris (2020). Dynamic rupture simulations of the M6. 4 and M7. 1 July 2019 Ridgecrest, California, earthquakes. Geophysical Research Letters, 47(7), e2019GL086020.

Magistrale, H., & Day, S. (1999). 3D simulations of multi-segment thrust fault rupture. *Geophysical Research Letters*, *26*(14), 2093-2096.

Matsu'ura, M. (1977). Inversion of geodetic data. Part II. Optimal model of conjugate fault system for the 1927 Tango earthquake. Journal of Physics of the Earth, 25(3), 233-255.

Oglesby, D. D. (2005). The dynamics of strike-slip step-overs with linking dip-slip faults: Bulletin of the Seismological Society of America, v. 95(5), p. 1604-1622, doi:10.1785/0120050058.

Oglesby, D. D. (2008). Rupture termination and jump on parallel offset faults: Bulletin of the Seismological Society of America, v. 98(1), p. 440-447, doi:10.1785/0120070163.

Ross, Z. E., B. Idini, Z. Jia, O. L. Stephenson, M. Zhong, X. Wang, Z. Zhan, M. Simons, E. J. Fielding, S. H. Yun, and E. Hauksson, E. (2019). Hierarchical interlocked orthogonal faulting in the 2019 Ridgecrest earthquake sequence. Science, *366*(6463), pp.346-351. doi:10.1126/science.aaz0109

Savage, J. C. (1965). The stopping phase on seismograms. *Bulletin of the Seismological Society of America*, *55*(1), 47-58.

Thatcher, W., and D. P. Hill (1991). Fault orientations in extensional and conjugate strike-slip environments and their implications. *Geology*, *19*(11), 1116-1120.

Wang, H., M. Liu, B. Duan, and J. Cao (2020). Rupture Propagation along Stepovers of Strike-Slip Faults: Effects of Initial Stress and Fault Geometry: Bulletin of the Seismological Society of America, v. 110(3), p. 1011-1024, doi:10.1785/0120190233.

Yue, H., T. Lay, and K. D. Koper (2012). En échelon and orthogonal fault ruptures of the 11 April 2012 great intraplate earthquakes. Nature, 490(7419), 245-249.